

# Structural and Photophysical Properties of Various Polypyridyl Ligands: A Combined Experimental and Computational Study

Liesbeth De Bruecker,<sup>[a]</sup> Jonas Everaert,<sup>[b]</sup> Pascal Van Der Voort,<sup>[c]</sup> Christian V. Stevens,<sup>[b]</sup> Michel Waroquier,<sup>[a]</sup> and Veronique Van Speybroeck\*<sup>[a]</sup>

Covalent triazine frameworks (CTFs) with polypyridyl ligands are very promising supports to anchor photocatalytic complexes. Herein, we investigate the photophysical properties of a series of ligands which vary by the extent of the aromatic system, the nitrogen content and their topologies to aid in selecting interesting building blocks for CTFs. Interestingly, some linkers have a rotational degree of freedom, allowing both a trans and cis structure, where only the latter allows anchoring. Therefore, the influence of the dihedral angle on the UV-Vis spectrum is studied. The photophysical properties are investigated by a combined computational and experimental study. Theoretically, both static and molecular dynamics simulations are performed

to deduce ground- and excited state properties based on density functional theory (DFT) and time-dependent DFT. The position of the main absorption peak shifts towards higher wavelengths for an increased size of the  $\pi$ -system and a higher  $\pi$ -electron deficiency. We found that the position of the main absorption peak among the different ligands studied in this work can amount to 271 nm; which has a significant impact on the photophysical properties of the ligands. This broad range of shifts allows modulation of the electronic structure by varying the ligands and may help in a rational design of efficient photocatalysts.

## 1. Introduction

One of the major challenges of today's society is how to provide materials and chemicals in a more sustainable and energy efficient way. Still today most of our energy resources originate from fossil fuels.<sup>[3]</sup> Sunlight is an abundantly available energy source and may provide sustainable opportunities for activating chemical reactions based on photocatalysis.<sup>[6,70,94,41,84,69,47,75]</sup> However, most of the currently used active photocatalytic homogeneous catalysts<sup>[69,61]</sup> necessitate an environmentally unfriendly cycle to remove the catalyst from the products. In this respect, it is important to develop recyclable and reusable heterogeneous photocatalysts, which can be achieved by anchoring the photocatalytic complexes on a porous framework. The step to remove the

catalyst can be avoided in this way and, as such, heterogeneous photocatalysis can serve as an environmentally cleaner alternative.<sup>[76,71,85,88]</sup>

Covalent organic frameworks (COFs) and covalent triazine frameworks (CTFs) are a relatively new class of materials with a large potential to be used as support materials for heterogeneous catalysis due to their high surface area<sup>[21]</sup> and tunability because of the availability of various building blocks.<sup>[53]</sup> Compared to other supports which have been explored for anchoring photocatalytic complexes such as metal organic frameworks,<sup>[35,38]</sup> they are more stable.<sup>[54,37,96]</sup> Interestingly, they also display (photo)catalytic activity in their pristine form<sup>[91,78,51]</sup> without even anchoring an active complex, and in this sense it is important to understand the electronic properties of the various building blocks of the CTF framework. A special branch of COFs and CTFs are those that contain polypyridyl ligands (Figure 1), as they allow for a stable secured anchoring of active complexes to the solid support.<sup>[90,58]</sup> In principle, a large variety of ligands can be used, creating a versatile platform to engineer supports for anchoring various active complexes. For the CTF-type materials, several N-heterocyclic systems have been synthesized, including (bi)pyridine,<sup>[65,40,39,66,82,44,4,68,32]</sup> ludidine<sup>[39]</sup> and pyrimidine<sup>[39]</sup> systems. We recently studied the anchoring of a Ru<sup>2+</sup>, octahedrally chelated by three bidentate polypyridyl ligands, on a biphenyl-based CTF where some of the biphenyl linkers are replaced with polypyridyl ones.<sup>[58,90]</sup> Furthermore, the anchoring of Ir(III) on a CTF containing bipyridine has been shown to be very promising for C–H borylation<sup>[82]</sup> and the post-metalated hexaazatrinaphthylene based CTF with a Cu(OAc)<sub>2</sub> complex can be utilized as an efficient heterogeneous catalyst

[a] L. De Bruecker, Prof. M. Waroquier, Prof. V. Van Speybroeck  
Center for Molecular Modeling (CMM), Ghent University, Technologiepark  
46, 9052 Zwijnaarde, Belgium  
E-mail: Veronique.VanSpeybroeck@UGent.be

[b] J. Everaert, Prof. C. V. Stevens  
Research Group SynBioC, Department of Green Chemistry and Technology,  
Faculty of Bioscience Engineering, Ghent University, Coupure Links 653,  
9000 Ghent, Belgium

[c] Prof. P. Van Der Voort  
Center for Ordered Materials, Organometallics and Catalysis (COMOC),  
Department of Inorganic and Physical Chemistry, Ghent University,  
Krijgslaan 281 (S3), 9000 Ghent, Belgium

Supporting information for this article is available on the WWW under  
<https://doi.org/10.1002/cphc.202000592>

© 2020 The Authors. Published by Wiley-VCH GmbH. This is an open access article under the terms of the Creative Commons Attribution Non-Commercial NoDerivs License, which permits use and distribution in any medium, provided the original work is properly cited, the use is non-commercial and no modifications or adaptations are made.

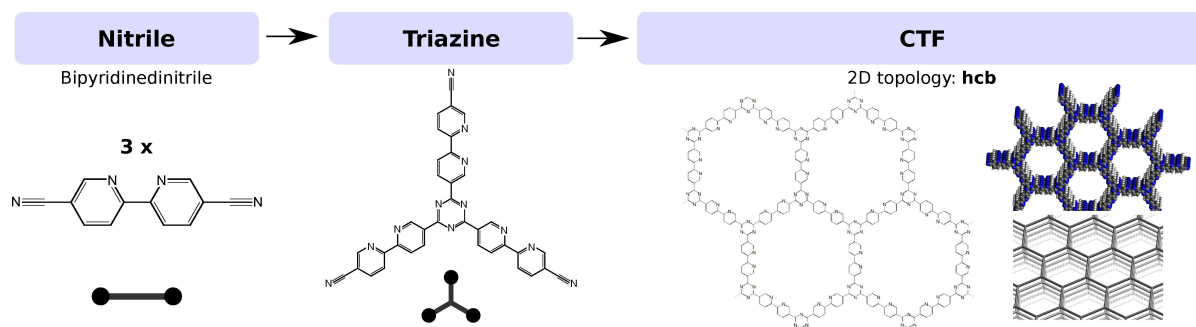


Figure 1. Synthesis of CTFs via cyclic trimerization of aromatic polypyridyls.

for the Henry reaction.<sup>[83]</sup> A review on this topic can be found in Ref. [81].

Driven by this application oriented goal, we ought it necessary to perform an in-depth investigation of the fundamental structural and photophysical properties of a series of polypyridyl ligands, which can eventually be used in a CTF scaffold. The considered nitrogen containing ligands are shown

in Figure 2. The box indicates the linkers which are experimentally characterized in this work. Note that most of the linkers are terminated by cyano groups to mimic the experimental conditions in which a CTF is synthesized by trimerization of linkers terminated by such groups as shown in Figure 1.<sup>[40]</sup> To make a proper comparison with literature data we also examined the pristine pyridine and bipyridine linker, which are

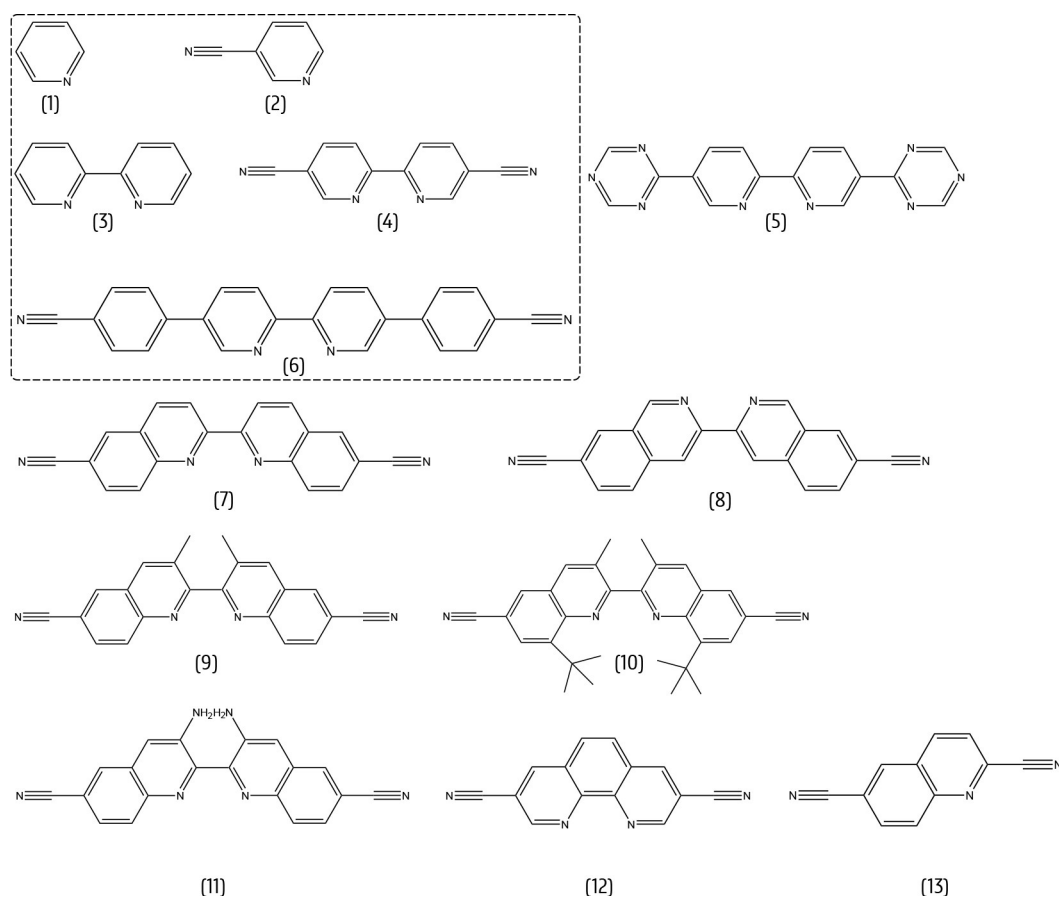


Figure 2. Polypyridyl ligands studied in this work: (1): pyridine (2): pyridine-3-carbonitrile (nicotinonitrile) (3): 2,2'-bipyridine (4): 2,2'-bipyridine-5,5'-dicarbonitrile (5): 5,5'-bis(4-cyanophenyl)-2,2'-bipyridine (6): 5,5'-bis(4-cyanophenyl)-2,2'-bipyridine (7): [2,2'-biquinoline]-6,6'-dicarbonitrile (8): [3,3'-biisoquinoline]-7,7'-dicarbonitrile (9): 3,3'-dimethyl-[2,2'-biquinoline]-6,6'-dicarbonitrile (10): 8,8'-di-tert-butyl-3,3'-dimethyl-[2,2'-biquinoline]-6,6'-dicarbonitrile (11): 3,3'-diamino-[2,2'-biquinoline]-6,6'-dicarbonitrile (12): phenantroline-5,5'-dicarbonitrile (13): quinoline-2,6-dicarbonitrile. The box indicates the linkers which are experimentally characterized in this work.

terminated by hydrogen atoms. For the bipyridine linker, we also investigated the influence of the termination group, which is the reason why we also included linker (5) terminated with triazine groups. We performed a combined theoretical and experimental study. Ligands (4), (6) and (13) were synthesized and together with ligands (1)–(3), their photophysical properties were characterized by means of UV-Vis spectroscopy. From a theoretical point of view, the structural and photophysical properties of all ligands were studied using both static and molecular dynamics (MD) based density functional theory (DFT) methods. We especially focused on the possible occurrence of both *cis*- and *trans* conformers, where the nitrogen atoms are either on the same or on opposite sides of two pyridine rings. The *trans* structure is energetically the most stable, but for anchoring of metal containing complexes the *cis* structure is preferred.<sup>[16,22,46]</sup> Furthermore we studied the influence of the dihedral angle on the UV-Vis spectrum calculated by means of time-dependent density functional theory (TDDFT) and performed a fundamental analysis of the most important electronic excitations. This theoretical study provides insight in the characterization of the excited states of the linkers and can in this way complement the experimental results. Earlier work showed that within a COF scaffold, the principle of orthogonal electronic structure engineering is valid, *i.e.*, the overall electronic structure can be tuned by independently varying the constituents.<sup>[90]</sup> This has been shown for the catalytic complex, but also extends to the combined complex-CTF catalyst. In this sense, a detailed insight is provided into how the electronic structure can be modulated by varying the ligands. Overall this study should give a guidance to design nitrogen containing CTFs and more in particular how the specific linker topology influences the optical properties.

## Computational details

In this work, the theoretical approach is based on both static and molecular dynamics simulations. All static calculations were performed with the Gaussian 16 software.<sup>[24]</sup> Geometrical optimizations and rotational scans were calculated using density functional theory (DFT). We checked that all computed internal normal modes of the optimized structures show positive frequencies, ensuring that the geometries represent minima of the ground state potential energy surface. Excited states were investigated adopting the time-dependent density functional theory (TDDFT) scheme,<sup>[72]</sup> within the linear-response approach as developed by Casida.<sup>[14]</sup> Electronic excitations are characterized by both the energies and oscillator strengths,<sup>[2]</sup> which correspond to peak positions and intensities of the transitions respectively. We convoluted the simulated spectra with a Gaussian envelope with a half-width at half height of 0.1 eV to simulate the Franck-Condon width of spectra. Solvent effects have been taken into account in the static and TDDFT calculations using a polarizable continuum model (PCM).<sup>[87]</sup> For the pyridine molecule, expressed by ligand (1), different functionals and basis sets have already been tested in literature,<sup>[23,64]</sup> revealing that B3LYP/6-31 + G\* yields good results. In all our calculations, we used the larger 6-31 + +G\*\* basis set. In accordance with what has been reported in literature, there is still a discrepancy between theory and experiment. No DFT level of theory is able to predict a correct state ordering of the low-energy excited states of pyridine, as observed in experiment.<sup>[8,92,30]</sup> Besides, we have used several

functionals coming from different rungs on Jacob's ladder<sup>[67]</sup> to test their performance in reproducing the structural properties of ligand (4): PBE<sup>[1]</sup> and BLYP<sup>[50,57]</sup> based on Generalized Gradient Approximation (GGA), B3LYP<sup>[7,51]</sup> as hybrid functional, the long-range corrected CAM-B3LYP,<sup>[95]</sup>  $\omega$ B97X-D,<sup>[15]</sup> LC- $\omega$ HPBE,<sup>[34]</sup> and the metahybrid M06<sup>[98]</sup> and TPSSH.<sup>[77,86]</sup> These functionals will also be used to compute the electronic excitations of bipyridine. Furthermore, we also studied the dependence on the choice of basis set for the calculation of the excited states.

The *ab initio* molecular dynamics (MD) simulations have been carried out with the CP2K software package (CP2K 3.0)<sup>[89]</sup> at the BLYP level of theory. The time step for integrating the equations of motion was set at 0.5 fs and the simulations were performed in the NVT ensemble at a temperature of 300 K. Grimme D3 dispersion corrections were included.<sup>[31]</sup>

Explicit information about the experimental details can be found in the Supporting Information.

## 2. Results and Discussion

We start with analyzing the experimental UV-Vis spectra of linkers (1)–(4) and (6) and explore the influence of extending the  $\pi$ -system and increasing the  $\pi$ -electron deficiency. After this we proceed with a computational study. As all linkers shown in Figure 2 are composed of one or more pyridine rings, we first investigate the ground and excited state properties of a pyridine molecule alone (ligand (1)), before exploring the more complex linkers. By comparing linkers (1) and (2), we examine the effect of adding a cyano group. Subsequently, we investigate the structural properties of linkers (3)–(8) which possess an additional rotational degree of freedom around the central axis. Biphenyl, being the most simple poly-cyclic aromatic hydrocarbon with this internal rotation, has been extensively studied in literature.<sup>[26,29,80]</sup> As the lone electron pairs of the nitrogen atoms will have a significant effect on the rotational profile of the energy, we preferred to take ligand (4) as study case for a thorough analysis as this compound is more representative for the polypyridyl linkers (3)–(10). At the same time, the influence of the internal rotation on the photophysical properties is investigated.

Complementary to a static approach, the sensitivity of the UV-Vis spectra to structural deformations has also been explored via a series of molecular dynamics (MD) calculations. This multi-step procedure has been introduced earlier by some of us.<sup>[36,20]</sup> Finally, we investigate the UV-Vis spectra of the other ligands which contain a varying amount of nitrogen atoms and which show different topologies of the aromatic rings in order to select the most promising structure for the construction of CTF scaffolds.

### 2.1. Experimental UV-Vis Spectra

The experimental spectra of linkers (1)–(4) and (6) are shown in Figure 3 along with the energies of the main absorption peaks. Two effects are studied. First, we analyze the influence of extending the  $\pi$ -system, which is achieved when more aromatic

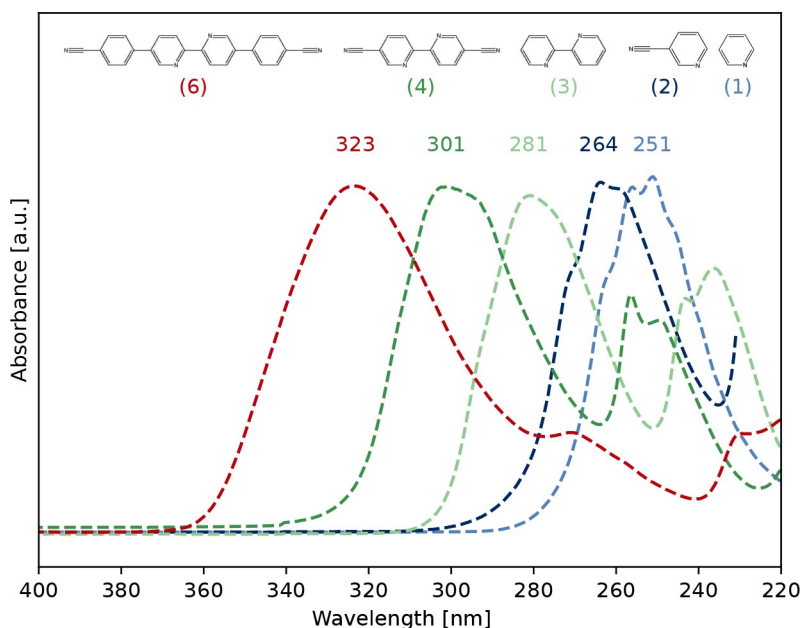


**Figure 3.** Experimental UV-Vis spectra of ligands (1)–(4) and (6) in acetonitrile as solvent. The energies of the main absorption peaks are indicated.

rings are added. Therefore, we compare linkers (1) and (3) on the one hand, and linkers (4) and (6) on the other hand. In both cases, the experiment predicts a shift towards larger wavelengths of 30 and 22 nm, respectively. This is indicated with green arrows in Figure 4. The experimental values are shown along with the computational results between parentheses, which will be discussed in Sections 3.2 and 3.4. The system is  $\pi$ -electron deficient due to the presence of nitrogen atoms as their free electron pairs are not part of the aromatic system and as a result, the linker will accept electrons more easily. Therefore, we also investigate the effect of increasing the  $\pi$ -electron deficiency. This can be done by adding electron-withdrawing groups such as the cyano group,  $\text{CN}^-$ . Its influence can be quantified by comparing the spectra of linkers (1) and (3) with those of linkers (2) and (4) respectively. In both cases, we observe a shift towards larger wavelengths: 13 nm and 20 nm, respectively, as shown in light blue in Figure 4. These shifts are in agreement with Ref. [90], in which it has been shown that the band gap decreases when the nitrogen content of the CTF

increases. Finally, by comparing linkers (2) and (4), we study the combined effect of increasing the size of the  $\pi$ -system and  $\pi$ -electron deficiency. We observe a large shift of 37 nm towards larger wavelengths. This is indicated in dark blue in Figure 4. The computational results will be discussed later.

### 3.2. Ground State and Excited State Properties of Pyridine and Nicotinonitrile

We will now proceed with the theoretical study. We start with pyridine as the smallest species of the N-hetero-aromatic family (ligand (1)) and which is regarded as reference system to tackle the more complex linkers. Several experimental studies<sup>[92,30,8]</sup> are devoted to pyridine and due to its small size and  $C_{2v}$  symmetry very accurate methods can be used to investigate this system computationally.<sup>[92,62,11,93,74,73,43,13,23]</sup> An extended benchmark study of the excitation energies in the pyridine ring has been done by Egidi et al.<sup>[23]</sup> This computational study uses a large set

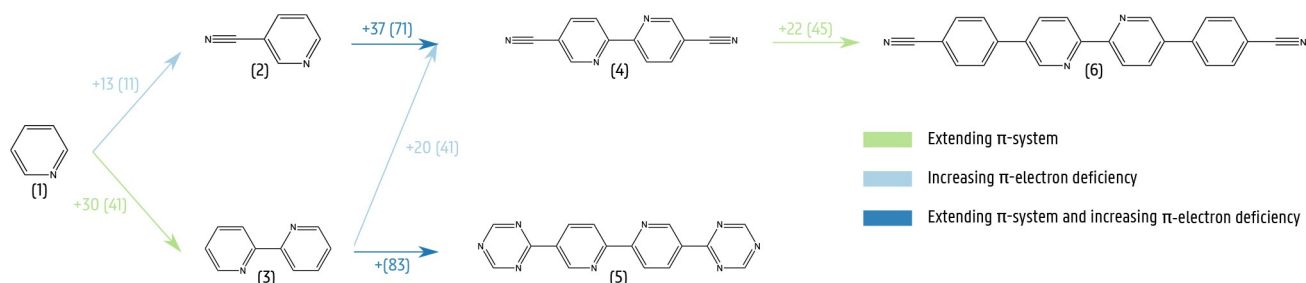


**Figure 4.** Influence of extending the  $\pi$ -system and increasing the  $\pi$ -electron deficiency of the linkers on the position of the main absorption peak. Shifts are given in nm. We report experimental results along with the computational findings between parentheses. The computational results are obtained at the B3LYP/6-31 + + G\*\* level of theory with acetonitrile as solvent and are discussed in Sections 3.2 and 3.4.

of multi-reference, coupled cluster singles and doubles (CCSD), and DFT methods. Contrary to the wave function based methodologies, TDDFT fails to reproduce the excited state ordering as observed in experiment,<sup>[92,30,8]</sup> for all tested functionals (B3LYP, CAM-B3LYP and M06-2X). The same failure of TDDFT has also been noticed for biphenyl.<sup>[26]</sup> It was found that PBE1PBE calculations significantly underestimated the excitation energy of the  $1^1B_1$  state because the dynamical and non-dynamical correlations are not considered appropriately. Indeed, it is known that TDDFT sometimes underestimates the energy differences of low-lying excited states of conjugated systems with several degenerate states such as porphyrines and fullerenes.<sup>[25,27,28]</sup>

In the following, we focus on the first three singlet excitations in pyridine, resulting from B3LYP/6-31 + +G\*\* calculations. As the ground state is a singlet, only singlet excitations can have a non-zero oscillator strength. This is due to the spin selection rule, which states that no change in the spin quantum number can occur.<sup>[33]</sup> This rule is strongly obeyed and can only be relaxed by effects that make the spin a poor quantum number like spin-orbit coupling. The molecular orbitals (MOs) involved in the first three singlet transitions are shown in Figure 5. The three highest occupied MOs (HOMO, HOMO-1, and HOMO-2) are displayed on the left in descending order and the unoccupied orbitals (LUMO and LUMO + 1) are displayed on the right. As their ordering can easily be switched by changing the level of theory or by extending the  $\pi$ -system, we therefore prefer to specify the levels with their true nature,

being  $n$ ,  $\pi_{AQ}$  or  $\pi_Q$ . The HOMO is a non-bonding orbital,  $n$ , whereas all others are  $\pi$ -orbitals, of which two quinoid (Q) and two antiquinoid (AQ) structures. This nomenclature is borrowed from the Jahn-Teller distorted benzene radical anion.<sup>[18]</sup> Placing an electron in a  $\pi_Q^*$  orbital causes a shortening of the lateral bonds, while placing it in a  $\pi_{AQ}^*$  orbital results in an elongation of those bonds. The transition with the lowest excitation energy involves an electron transfer from the  $n$ -orbital to  $\pi_Q^*$  and is indicated with a blue arrow in Figure 5. For the second transition, presented in black, an  $n \rightarrow \pi_{AQ}^*$  excitation takes place. This transition is dark, *i.e.*, the oscillator strength,  $f$ , = 0. The third transition, indicated in green, is the brightest one with  $f = 0.0382$  and corresponds to the highest peak in the UV-Vis spectrum. It has two contributions, namely  $\pi_{AQ} \rightarrow \pi_{AQ}^*$  and  $\pi_Q \rightarrow \pi_Q^*$ . In the case when the transition has multiple non-negligible contributions, the strongest components are taken up in the figure accompanied by their corresponding amplitude in square brackets. It implies that the 229 nm peak mainly consists of a strong  $\pi_Q \rightarrow \pi_Q^*$  transition with an amplitude of 0.64 and a less significant  $\pi_{AQ} \rightarrow \pi_{AQ}^*$  transition with an amplitude of 0.29. This mix of local transitions in the dominant excitation peak is also reported by Egidi et al.<sup>[23]</sup> The darkness of the second transition at 234 nm can be explained based on symmetry rules. As shown in the Supporting Information, the symmetry of the excited state must equal the symmetry of one of the components of the dipole moment operator. Pyridine belongs to the  $C_{2v}$  symmetry point group and the orbitals shown in Figure 5 have  $B_1$ ,  $A_2$ ,  $A_1$ ,  $B_1$ , and  $A_2$  symmetry in order

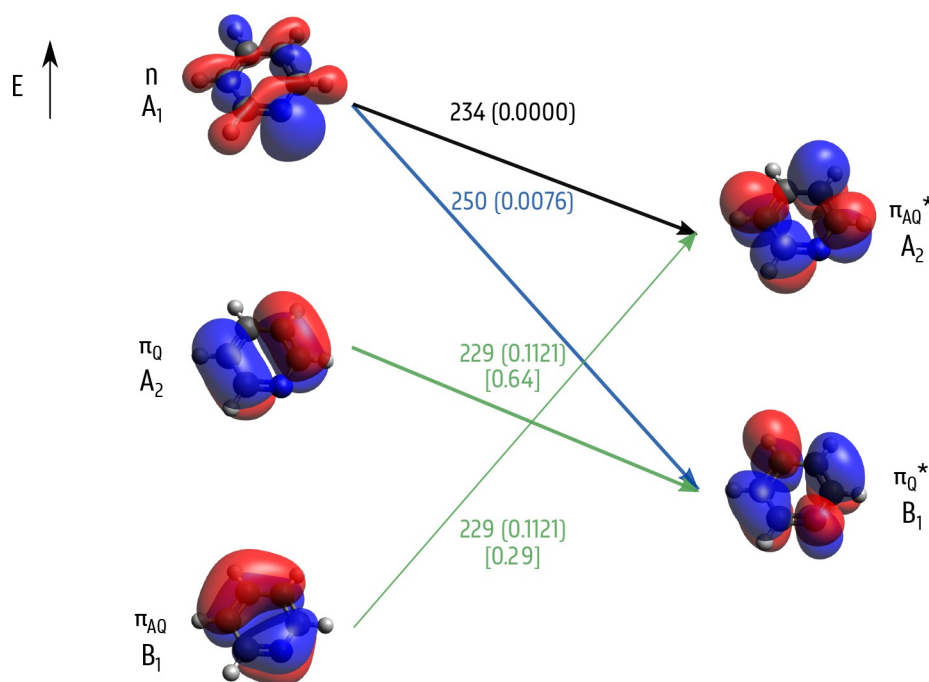


**Figure 5.** Visualization of the important orbitals of pyridine (1) along with their symmetry labels. The arrows indicate the most dominant contributions of the first three singlet excitations, characterized by the excitation energy in nm, oscillator strength,  $f$ , between brackets, and amplitude in square brackets if more contributions are reported for a specific excitation. The occupied MOs in the left represent respectively the HOMO, HOMO-1 and HOMO-2 in descending order. The unoccupied MOs in the right represent respectively the LUMO + 1 and LUMO. This labeling is conform the binding energies taken up in Table S1. The transition with the lowest excitation energy is indicated with a blue arrow, the dark transition is presented in black and the brightest transition is indicated in green. Calculations carried out at the B3LYP/6-31 + +G\*\* level of theory and with acetonitrile as solvent.

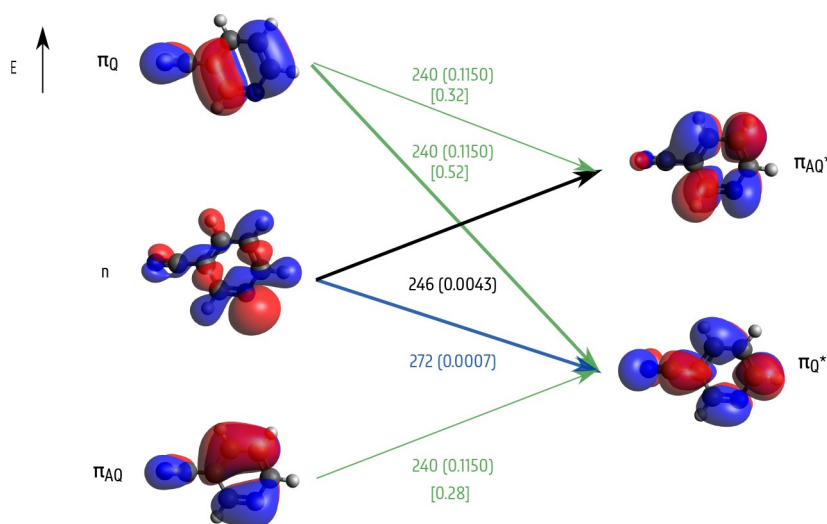


**Figure 6.** Visualization of the important orbitals of linker (2). The arrows indicate the most dominant contributions of the first three singlet excitations, characterized by the excitation energy in nm, oscillator strength,  $f$ , between parentheses, and amplitude in square brackets if more contributions are reported for a specific excitation. The occupied MOs in the left represent respectively the HOMO, HOMO-1 and HOMO-2 in descending order. The unoccupied MOs in the right represent respectively the LUMO + 1 and LUMO. This labeling is conform the binding energies taken up in Table S1. The transition with the lowest excitation energy is indicated with a blue arrow, the dark transition is presented in black and the brightest transition is indicated in green. Calculations carried out at the B3LYP/6-31++G\*\* level of theory and with acetonitrile as solvent.

of ascending energy. The dipole moment operator components have the  $B_1$ ,  $B_2$ , and  $A_1$  symmetries.<sup>[33]</sup> Therefore, the second transition is forbidden as the product of  $A_1$  and  $A_2$  is  $A_2$ . Relaxation of this rule is possible by vibronic coupling, which we will not study in this paper.

The binding energies of some relevant MOs are reported for the series of ligands (1)–(6) in Table S1 of the Supporting Information. The nature of these orbitals is also given, and it is indicated how the binding energy of these orbitals with a certain nature changes in terms of the specific structure of the ligands. We can now easily investigate the effect of adding a cyano group and thus increasing the  $\pi$ -electron deficiency of the system, by comparing the UV-Vis spectra of ligands (1) and (2). The isosurfaces of the orbitals involved in the most dominant contributions of the first three singlet excitations of linker (2) are shown in Figure 6 and can be compared to those of linker (1) shown in Figure 5. We notice that the  $n$ -orbital is now lower in energy than  $\pi_Q$ , although the difference is very small (see Table S1), and that it is no longer figuring as HOMO. Furthermore, the orbitals of  $\pi_Q^*$  and  $\pi_{AQ}^*$  are rotated clockwise over one atom when  $CN^-$  is added. Based on the nature of the orbitals, we notice that the characteristics of the first three excitations of ligand (2) are the same as in pyridine. The only difference is the smaller contribution of the main absorption peak at 240 nm, but the largest contribution is identical. Furthermore, the second peak at 246 nm is not dark, in contrary to what has been observed in pyridine. This is because the symmetry group is reduced, namely from  $C_{2v}$  to  $C_s$ , and therefore there are no symmetry forbidden transitions. Indeed, in the  $C_s$  symmetry group, the dipole moment operator components have  $A'$  and  $A''$  symmetry, and thus every transition is electric-dipole allowed.

The theoretical and experimental UV-Vis spectra of linkers (1) and (2) are shown in Figure 7. Although there is a significant

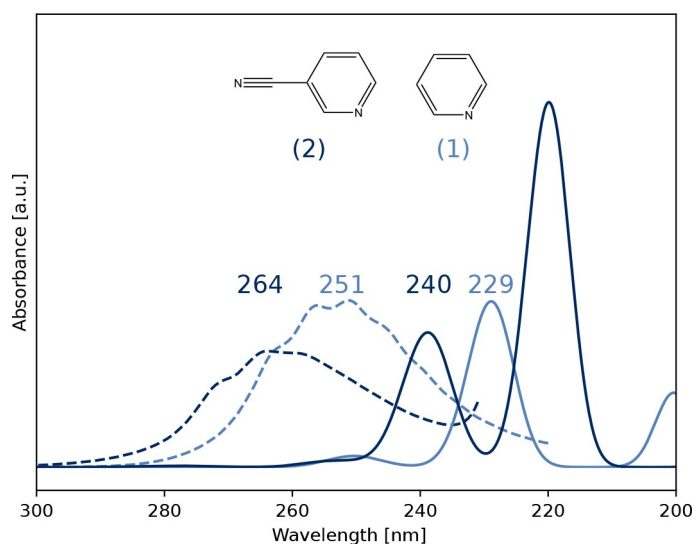


**Figure 7.** Theoretical (full lines) and experimental (dashed lines) UV-Vis absorbance spectra of ligands (1) and (2). Calculations carried out at the B3LYP/6-31++G\*\* level of theory and with acetonitrile as solvent.

shift between theory and experiment, which has also been observed in Ref. [23], the calculations confirm the experimentally observed shift towards higher wavelengths when  $CN^-$  is added. The calculated shift is 11 nm for the bright excited state, which is in excellent agreement with the experimental shift of 13 nm as shown in Figure 4.

Our calculations on these reference systems show that the addition of a cyano group results in a shift of the main absorption peak towards larger wavelengths and confirm our experimental results.

### 3.3. Structural Properties of Polypyridyl Ligands

After analyzing the photophysical properties of the reference systems (1) and (2), we study several polypyridyl ligands which are promising for the construction of CTF scaffolds as shown in Figure 1. Before we investigate the excited state properties, we perform an in-depth analysis of the structure of the ligands exhibiting a rotational degree of freedom around the central bond, *i.e.*, linkers (3)–(8). This rotation is characterized by the dihedral angle shown in Figure 8. In order to perform a rotational scan, we start with an optimized cis conformer, after which we vary the dihedral angle with a step size of  $10^\circ$ . At every step, the structure is fully optimized except for the frozen dihedral. A schematic representation of the rotational profile, relative to the trans configuration, is shown in Figure 9. Two minima are observed as the ligands have two (meta)stable conformers, namely trans and cis. In the trans conformation, characterized by a dihedral angle of  $180^\circ$ , the nitrogen atoms are at opposite sides of the bond between the two pyridine rings, while in cis the nitrogen atoms are at the same side of the bond, corresponding to a dihedral angle  $\phi_{cis}$ . The conformational equilibrium is determined by conjugation of the two  $\pi$ -systems, steric hindrance by the hydrogen atoms and electrostatic interactions.<sup>[29,45]</sup> The trans conformer is predicted to be lower in energy than the cis conformer. The reason for this is that the repulsive interaction between the lone-pair

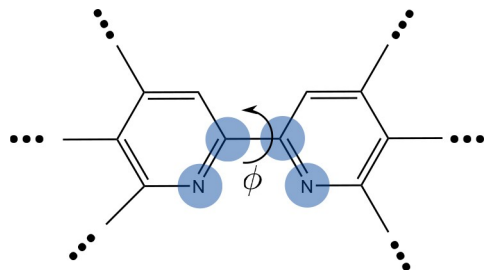


Figure 8. Schematic representation of the dihedral angle  $\phi$  in a polypyridyl ligand.

electrons of the nitrogen atoms is smaller than the attractive interactions between a nitrogen and a hydrogen atom situated on different rings.

Now we focus on linker (4), for which we discuss the rotational profile in detail and test the performance of various levels of theory. The trans conformer is the most stable structure, both in the gas phase as with acetonitrile as solvent. This is in agreement with literature data found for bipyridine where it has been reported that the trans conformer is also present in organic solvents and in basic or very strong acidic environment.<sup>[60]</sup> Furthermore, results of X-ray analysis indicate that the molecule has a trans configuration in the crystalline state.<sup>[55]</sup> The trans configuration is found to be planar in our theoretical calculation, which is in agreement with Ref. [55]. However, dipole moment measurements in organic solvents and in basic solutions indicate a non-planar trans configuration, with a dihedral angle of  $20^\circ$ .<sup>[17]</sup> This discrepancy has been studied before. As the non-planarity was not due to the lack of electron correlation during the optimization,<sup>[63]</sup> it has been shown that the solvent-solute interactions lie on the basis for this deviation. However, we observe a planar trans conformation in our static calculations in which solvent is included using PCM.

On the other hand, the cis form has not yet been observed in its isolated form. Only in some specific environments it appears that the cis conformation indeed exists and even prevails. So are metal-chelate compounds<sup>[22,46,16]</sup> and mono-cation structures of bipyridine favoring the cis-form.<sup>[60,19]</sup> Also compounds forming an adduct with typical Lewis acceptors such as  $\text{SbCl}_3$ ,  $\text{AsCl}_3$ ,  $\text{BiCl}_3$ <sup>[52,12,9]</sup> or embedded in phosphinic centers<sup>[10]</sup> appear as stable structures with the bipyridine in a cis conformation. The cis structure is not planar, which is caused by the steric hindering between the extended non-bonding orbitals of the nitrogen atoms. However, when embedded in a transition metal complex, the linker is planar.<sup>[58]</sup> The large difference in the permanent dipole moment between the cis and trans conformers means that not only chelating and protonation effects, but that also pure electrostatic interactions contribute to the stabilization of the cis structure.

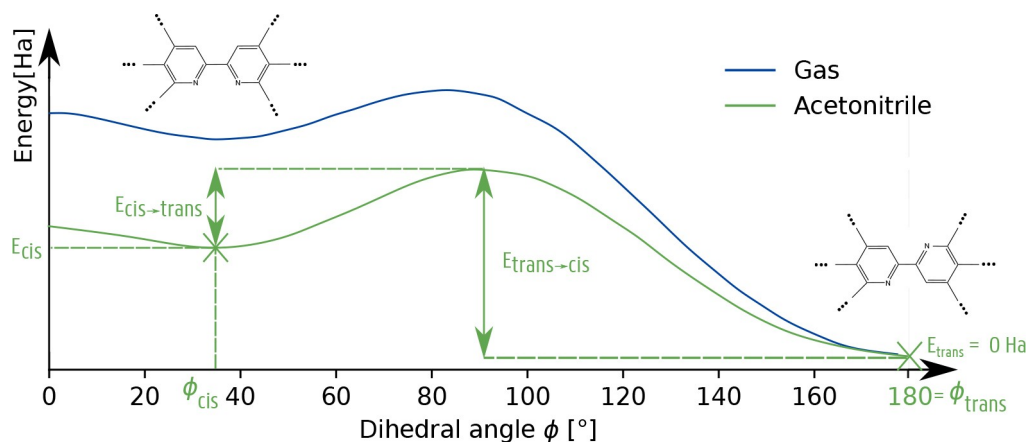


Figure 9. Schematic representation of the torsional potential energy curve for the relaxed ground state, both in the gas phase and in solvent. The two (meta) stable conformers are indicated.

We now examine the dependence of  $\phi_{cis}$  on the selected DFT method. This structural parameter may vary in a relatively wide window ( $30^\circ$ – $43^\circ$ ) as shown in Table 1. The long-range corrected functionals, CAM-B3LYP,  $\omega$ B97X-D and LC- $\omega$ HPBE, yield significant larger  $\phi_{cis}$  values compared to the other functionals. Furthermore, it is not surprising that the dihedral angle is strongly correlated with the energy difference between the trans and cis structures,  $E_{cis}$ , and with the barrier  $E_{trans\rightarrow cis}$ , which has to be overcome to go from the trans to the cis configuration (Figure 9). These energies are also tabulated in Table 1. Values of  $E_{cis}$  are not varying much with the choice of functional. Larger deviations are observed for the barrier  $E_{trans\rightarrow cis}$  and obviously for  $E_{cis\rightarrow trans} = E_{trans\rightarrow cis} - E_{cis}$  too, *i.e.*, the barrier which has to be overcome to go from the cis to trans structure. The smallest barriers are noticed for the long-range corrected functionals. Other structural parameters of the geometry of the trans structure of ligand (4) are tabulated in Table S2 of the Supporting Information. Only results for B3LYP and M06 are shown as the other functionals are inferior for the description of the excited states as will be shown in Section 3.4. Both for organic and inorganic molecules, M06 performs particularly well.<sup>[42,49]</sup> We may generally conclude that the influence of the level of theory on the geometrical parameters of the trans configuration is negligibly small.

The influence of solvent on the energetics is large as can be seen in Figure 9 and Table 1. The results reported in Table 1 are obtained with acetonitrile, which has a relative permittivity of  $\epsilon_r = 37.5$ . The barrier  $E_{trans\rightarrow cis}$  decreases with at least 10 kJ/mol, resulting in an increase of the probability of finding the ligand in the cis conformation. This is in agreement with the findings of Ref. [45] where the authors report an increase of the dipole moment when  $\epsilon_r$  increases. The larger dipole moment is attributed to a higher population of the dipolar cis structure.

To support these findings, we performed a series of molecular dynamics (MD) simulations at 300 K and checked if a transition from the trans to cis structure or vice versa takes place. In Figure 10, the histograms are shown for the dihedral angles encountered in the MD simulations from the trans to cis conformer (left) and vice versa (right). When starting in the trans conformer, we do not observe any transition after 53 ps. In the inset of the left pane of Figure 10, it is shown that the peak of the trans conformer is situated at  $175^\circ$  instead of at  $180^\circ$  as we would expect from the geometry optimizations. This confirms the non-planar trans configuration with a dihedral angle of  $20^\circ$  observed in experiments.<sup>[17]</sup> When starting from the cis conformer, we see a transition to the trans conformer after 48 ps. After this, the linker remains in the trans conformer and no transition back to the cis structure has been observed

**Table 1.**  $\phi_{cis}$ ,  $E_{cis}$ ,  $E_{trans\rightarrow cis}$ , and  $E_{cis\rightarrow trans}$  for ligand (4), both with and without acetonitrile as solvent. Energies are given in kJ/mol and angles in  $^\circ$ . Calculations carried out at the B3LYP/6-31++G\*\* level of theory.

| Functional        | Without solvent |           |                            |                            | With solvent |           |                            |                            |
|-------------------|-----------------|-----------|----------------------------|----------------------------|--------------|-----------|----------------------------|----------------------------|
|                   | $\phi_{cis}$    | $E_{cis}$ | $E_{trans\rightarrow cis}$ | $E_{cis\rightarrow trans}$ | $\phi_{cis}$ | $E_{cis}$ | $E_{trans\rightarrow cis}$ | $E_{cis\rightarrow trans}$ |
| PBE               | 32.6            | 28.31     | 37.16                      | 8.85                       | 29.7         | 14.48     | 27.13                      | 12.65                      |
| BLYP              | 34.0            | 27.71     | 35.25                      | 7.54                       | 30.8         | 13.85     | 25.23                      | 11.38                      |
| B3LYP             | 35.7            | 28.69     | 35.58                      | 6.89                       | 32.4         | 14.33     | 25.14                      | 10.81                      |
| M06               | 34.7            | 28.67     | 37.32                      | 8.65                       | 31.8         | 14.49     | 27.05                      | 12.56                      |
| TPSSH             | 33.0            | 29.18     | 37.49                      | 8.31                       | 29.9         | 14.95     | 27.18                      | 12.23                      |
| CAM-B3LYP         | 39.5            | 28.92     | 33.92                      | 5.00                       | 36.1         | 14.04     | 22.69                      | 8.65                       |
| $\omega$ B97X-D   | 40.9            | 27.48     | 33.31                      | 5.83                       | 38.1         | 12.81     | 21.05                      | 8.24                       |
| LC- $\omega$ HPBE | 42.5            | 27.76     | 33.92                      | 6.16                       | 39.2         | 13.02     | 20.63                      | 7.61                       |

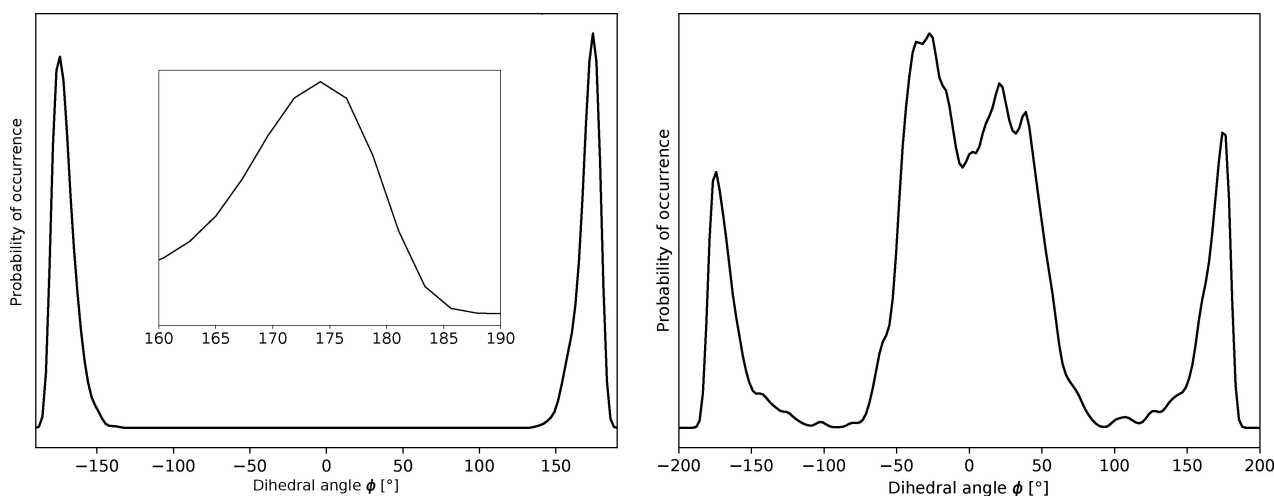


**Figure 10.** Histogram of the dihedral angle for the MD simulations starting from the trans conformer (left) and cis conformer (right) of linker (4). In the left pane, we zoomed in on the range between  $160^\circ$  and  $190^\circ$ . Calculations carried out at the BLYP level of theory.



after 100 ps. These results are expected, considering the rather high values for  $E_{cis}$  and  $E_{trans \rightarrow cis}$  reported in Table 1. The MD calculations were performed at the BLYP level of theory and in gas phase, however, the overall qualitative picture is expected to remain unaltered when solvent is taken into account.

Next, we study the influence of various terminations of the bipyridine linker on the energy profile, inspired by the synthesis conditions of the CTF scaffold. The results are shown in Table 2. Therefore we examine linkers (3)–(5) with H, CN<sup>-</sup>, and triazine as termination group respectively. Compared to the pristine bipyridine linker,  $E_{cis}$  and  $E_{trans \rightarrow cis}$  are slightly increased for a cyano- or triazine group termination. In addition,  $\phi_{cis}$  is larger. Bipyridine (linker (3)) has been studied extensively in literature and we find a good correspondence between our values and literature data (see Table S3). Table 2 also reports  $E_{cis'}$ ,  $\phi_{cis'}$ ,  $E_{trans \rightarrow cis'}$ , and  $E_{cis \rightarrow trans}$  for the other ligands with a rotational degree of freedom and we do not observe large differences between them. We mention the presence of an extra rotational degree of freedom of linker (6), *i.e.*, the rotation between the pyridine and benzene ring. However, this angle changes with less than 2° when a rotational scan is performed for  $\phi$ , the dihedral angle between the two pyridine rings.

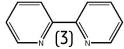
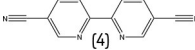
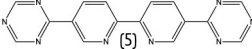
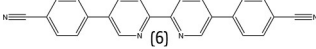
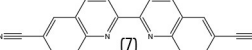
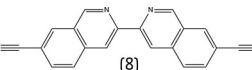
### 3.4. Excited State Properties of Polypyridyl Ligands

#### 3.4.1. Influence of Level of Theory on Excited State Properties

After studying the ground state properties, we investigate the electronic excitation spectra. First of all, we study the influence of the chosen functional on the UV-Vis spectrum of the trans

conformer of linker (4). The resulting calculated spectra are compared with experiment in Figure 11. As expected, the lack of including Hartree-Fock exchange in PBE results in a spectrum which needs a significant blue-shift to match the experimental data.<sup>[56,59]</sup> Contrarily, the long-range corrected functionals, shown in red, require a large red-shift, which is in agreement with earlier studies on compounds ranging from MOFs<sup>[36]</sup> to noble metal nanoclusters.<sup>[59]</sup> The best correspondence between theory and experiment is found for B3LYP and M06, for which the excitation energies of the two absorption peaks are indicated in Figure 11 along with the experimental values. Also the dependence on the choice of the basis set has been studied (see Figure S10): the UV-Vis spectrum varies only slightly. As no reference data has been found in literature for linker (4), we compare the calculated spectrum of the extensively studied linker (3) with experimental and computational literature data in order to test the chosen level of theory. Table S4 of the Supporting Information shows the structural parameters of the trans conformer of linker (3) from literature data and our calculations. In Table 3, the energies for the visible absorption peaks for the trans conformer of linker (3) are reported. Experimental studies reveal two absorption bands at 279 and 232 nm.<sup>[60]</sup> In Ref. [79] an overview is given of other experimental results. The gas phase UV-Vis spectrum has been calculated at the PBE1PBE/6-31 + G\*\* level of theory in Ref. [48], in which two intense transitions at 265 and 227 nm are observed. We conclude that B3LYP and M06 perform equally well and in the remainder of this paper we will systematically employ B3LYP as functional. Remark that those calculations were performed in the gas phase in contrast to the previous simulations in order to be comparable with the literature.

**Table 2.**  $\phi_{cis}$ ,  $E_{cis}$ ,  $E_{trans \rightarrow cis}$ , and  $E_{cis \rightarrow trans}$  for linkers (3)–(8). Energies are given in kJ/mol and angles in °. Calculations carried out at the B3LYP/6-31 + G\*\* level of theory and with acetonitrile as solvent.

| Ligand  | $\phi_{cis}$ | $E_{cis}$ | $E_{trans \rightarrow cis}$ | $E_{cis \rightarrow trans}$ |
|---|--------------|-----------|-----------------------------|-----------------------------|
|  | 34.2         | 11.97     | 20.86                       | 8.89                        |
|  | 32.4         | 14.33     | 25.14                       | 10.81                       |
|  | 33.3         | 13.77     | 24.46                       | 10.69                       |
|  | 32.8         | 13.19     | 24.09                       | 10.90                       |
|  | 34.2         | 14.94     | 24.11                       | 9.17                        |
|  | 36.4         | 14.20     | 25.74                       | 11.54                       |

**Table 3.** Energies of the visible absorption peaks [nm] and oscillator strength,  $f$ , between parentheses of the trans conformer of linker (3). Own calculations and literature data, both computational and experimental, are compared. Calculations are performed in the gas phase.

| Level of theory                    | Electronic excitations |              |             |
|------------------------------------|------------------------|--------------|-------------|
| B3LYP/6-31 + G**                   | 272 (0.465)            | 233 (0.061)  | 209 (0.065) |
| M06/6-311 + G**                    | 273 (0.456)            | 233 (0.0366) | 210 (0.051) |
| PBE1PBE/6-31 + G** <sup>[98]</sup> | 265 (0.485)            | 227 (0.057)  | 201 (0.080) |
| Experiment <sup>[63]</sup>         | 279                    | 232          |             |

Before continuing with the analysis of the UV-Vis spectrum, we briefly discuss the influence of the solvent on the excitation spectra. The results of linker (4) are shown in Table S5 of the Supporting Information. When solvent is included, we observe a shift of 5–9 nm towards larger wavelengths compared to the gas phase results.

We now examine the UV-Vis spectrum of linker (4) in detail. Figure 12 visualizes the orbitals involved in the most dominant contributions of the first non-dark and two bright excitations. They have the same character as the orbitals of ligand (2) shown in Figure 6. The first non-dark and first bright excitation are identical to these of linker (2) involving an  $n \rightarrow \pi_Q^*$  and  $\pi_Q \rightarrow \pi_Q^*$  excitation, respectively. The second bright excitation appears at a smaller wavelength (248 nm), has a much lower oscillator strength ( $f=0.0837$ ) and involves the following transitions:  $\pi_{AQ} \rightarrow \pi_Q^*$  and  $\pi_Q \rightarrow \pi_{AQ}^*$ . Furthermore, we studied the differences in geometry between the ground and relaxed excited state structures as shown in Table S6 of the Supporting Information. We remark that for the excited states the distance between the two rings decreases.

### 3.4.2. Influence of Extending $\pi$ -system and Increasing $\pi$ -electron Deficiency

The ligands in the series (1)–(6) show an increasing  $\pi$ -electron deficiency by adding a cyano group,  $CN^-$ , or an aromatic ring containing nitrogen atoms as termination group as demonstrated in Figure 4. Addition of aromatic rings to the chain extends the  $\pi$ -system. The theoretical UV-Vis spectra for this series of linkers are displayed in Figure 13. We observe that the larger the termination group, going from linker (3) over (4) to (5), the larger the shift of the highest peak towards longer wavelengths. This confirms the experimental results of Section 3.1. The MOs involved in the important excitations of linker (4), (3) and (5) are shown in Figure 12 and Figures S11 and S12 of the Supporting Information respectively. The character of all orbitals is identical and the contributing transitions to the first and two bright excitations are the same. Compared to linkers (3) and (4), the state ordering is interchanged for linker (5): for the former, the brightest transition is the second one, whereas it is the first for linker (5). However, we note that the excitation energies of the first two transitions lie very close to each other for linker (5). The energy shift of the bright excitation between linker (3) to (4) is circa 41 nm, where a shift of 20 nm has been observed experimentally as shown in Figure 4.

The influence of extending the  $\pi$ -system is best studied by comparing linkers (1) and (3) on the one hand and (4) and (6) on the other hand. The main absorption peak for linkers (1) and (3) shifts 41 nm (see Figure 11), which is larger than the experimental shift of 30 nm. A similar shift is noticed between ligands (4) and (6) (45 nm), which again is an overestimation with respect to experiment (shift of 22 nm).

By comparing the shifts between ligands (2) and (4), and between (3) and (5), we can study the combined effect of an extended  $\pi$ -system which is also more  $\pi$ -electron deficient. For both cases, we observe a large shift of 71 and 83 nm

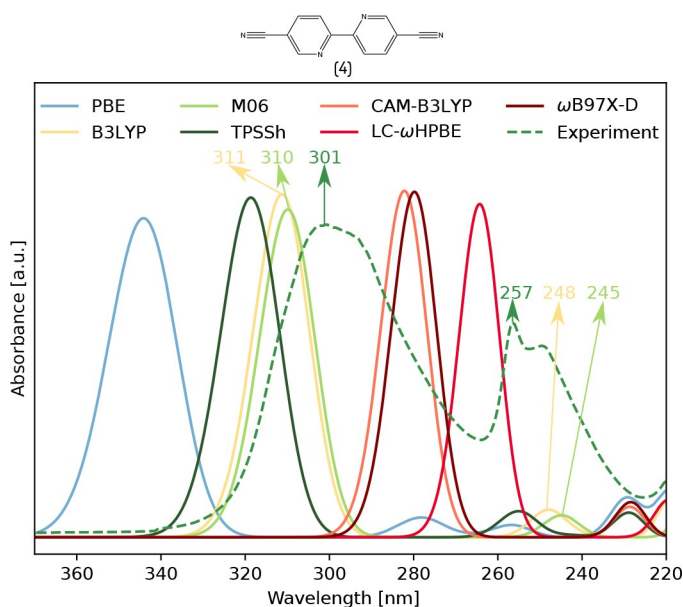


**Figure 11.** UV-Vis spectra of ligand (4) for several functionals (full lines) together with the experimental spectrum (dashed line). The energies of the first and second absorption peak are indicated for B3LYP, M06, and experiment. Calculations carried out with the 6-31++G\*\* basis set and with acetonitrile as solvent.

respectively as can be extracted from Figure 11. For completeness, the orbitals involved in the main absorption peak of linker (6) are shown in Figure S13 of the Supporting Information. The characters of the HOMO and LUMO are identical to these of the previously described linkers.

### 3.4.3. Influence of Dihedral Angle on Excited State Properties

In the previous subsections, we limited the excited state calculations by assuming that the system is in the energetically most favorable trans configuration corresponding with a dihedral angle of  $\phi=180^\circ$ . As some polypyridyl ligands favor the cis conformation in some specific environments, we extend this study by investigating the influence of the dihedral angle on the UV-Vis spectrum. As reference compound we consider ligand (4) for which experimental data are available in the literature. Structural properties have also been investigated theoretically in this study and have been discussed in Section 3.3. At the B3LYP/6-31++G\*\* level, a metastable cis conformation is found at  $\phi_{cis}=35.7^\circ$ . The UV-Vis spectrum is calculated for each point of the rotational scan and displayed in Figure 14 for some specific values of the dihedral angle.

We start the analysis from the planar trans conformer with a dihedral angle of  $180^\circ$ . The brightest transition is situated at high wavelengths, corresponding to a low excitation energy. When  $\phi$  decreases, the peak shifts to smaller wavelengths and thus the excitation energy increases. Meanwhile the conjugated  $\pi$ -system decreases when the structure becomes less and less planar as the  $\pi$ -interactions along the bond get weaker. Furthermore, the oscillator strength decreases. The lowest

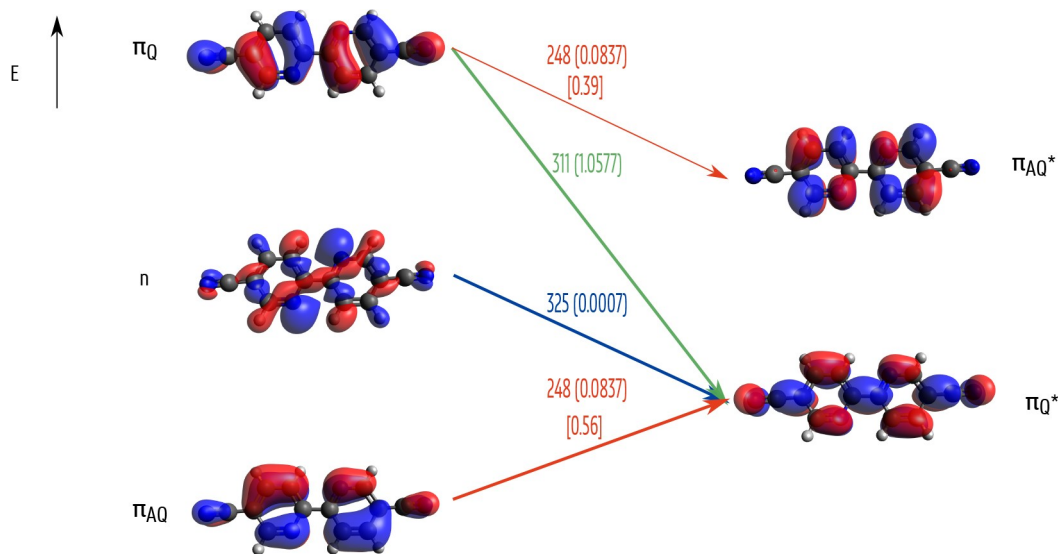


**Figure 12.** Visualization of the important orbitals of linker (4). The arrows indicate the most dominant contributions of the first non-dark and two bright excitations, characterized by the excitation energy in nm, oscillator strength,  $f$ , between parentheses, and amplitude in square brackets if more contributions are reported for a specific excitation. The occupied MOs in the left represent respectively the HOMO, HOMO-1 and HOMO-5 in descending order. The unoccupied MOs in the right represent respectively the LUMO+3 and LUMO. This labeling is conform the binding energies taken up in Table S1. The transition with the lowest excitation energy is indicated with a blue arrow and the first and second bright transitions are represented with green and red respectively. Calculations carried out at the B3LYP/6-31++G\*\* level of theory and with acetonitrile as solvent.

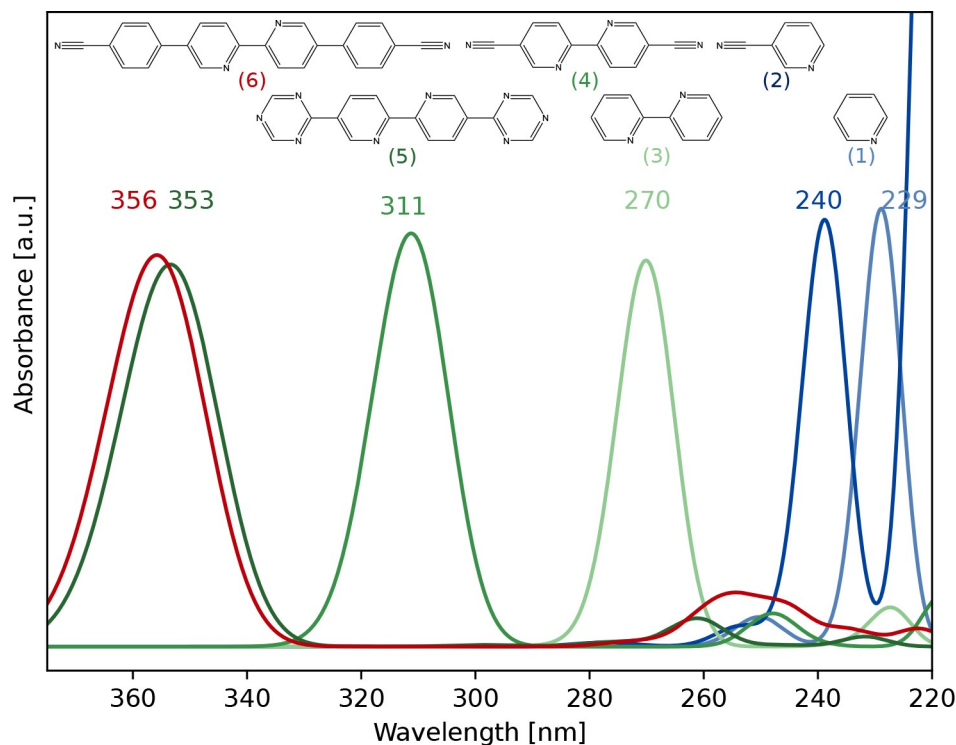


**Figure 13.** Theoretical UV-Vis spectra of ligands (1)–(6). The energies of the main absorption peak are indicated. Calculations carried out at the B3LYP/6-31++G\*\* level of theory and with acetonitrile as solvent.

wavelength is observed for structures with a dihedral angle of  $92^\circ$ . Then the spectrum closely resembles that of linker (2) as shown by the dotted black line. Indeed, the orbitals in the two rings are only slightly connected and the spectrum of linker (4)

is just the sum of its components, *i.e.*, linker (2). The dominant absorption peak of ligand (4) comes from a  $\pi_Q \rightarrow \pi_Q^*$  transition, which, in this compound, corresponds with a HOMO  $\rightarrow$  LUMO excitation as demonstrated in Figure 12 for the

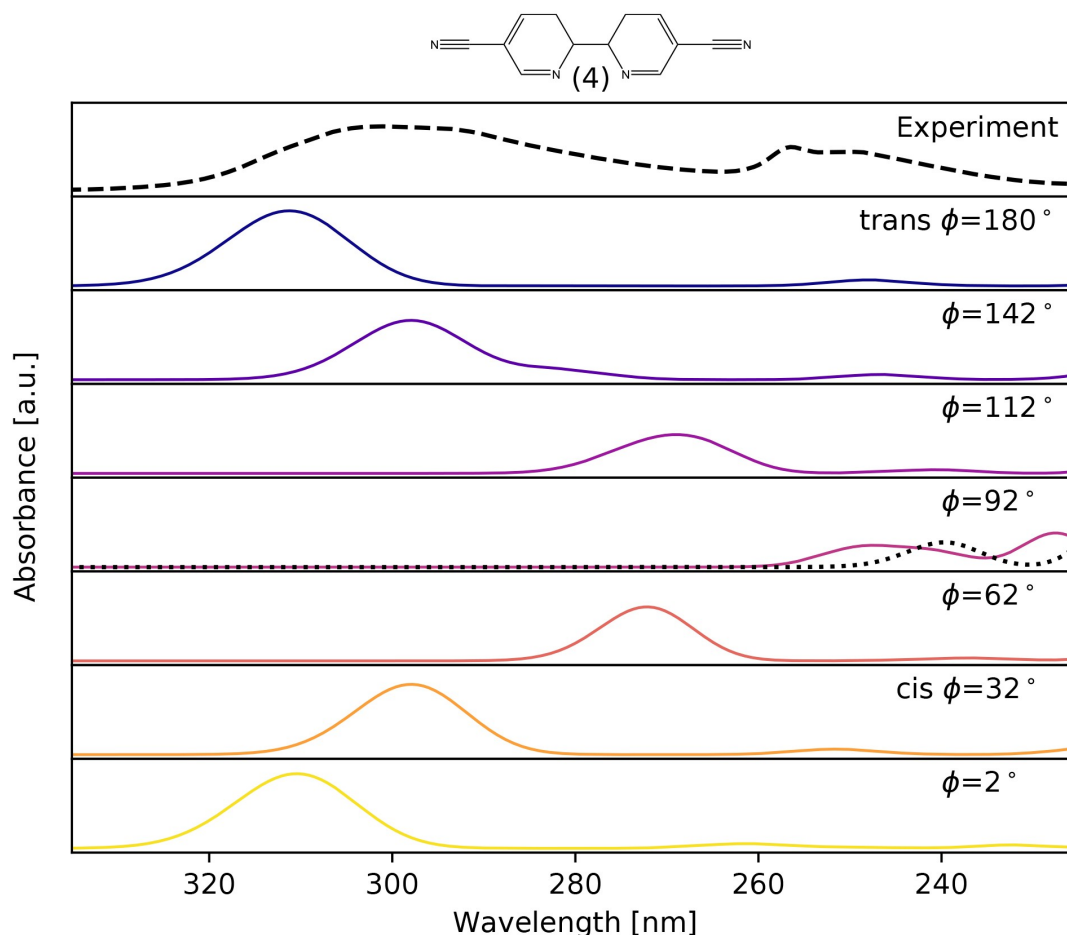


**Figure 14.** Influence of the dihedral angle on the UV-Vis spectrum of ligand (4). The experimental spectrum is indicated with a dashed line and the dotted line represents the spectrum of linker (2). Calculations carried out at the B3LYP/6-31++G\*\* level of theory and with acetonitrile as solvent.

trans structure. For a dihedral angle of  $92^\circ$ , the MOs are shown in Figure S14 of the Supporting Information. When  $\phi$  decreases further, the peak shifts to larger wavelengths again. This is accompanied by an increase of  $f$  as the conjugated  $\pi$ -system increases again when the structure becomes more planar. So the largest conjugated system has the smallest excitation energy, which is in agreement with Ref. [80]. The observed shift between planar and non-planar structures is 50 nm. Special attention is devoted to the cis conformer which is shown in orange. The orbitals involved in the most important transitions of the cis conformer are shown in Figure S15 of the Supporting Information and are compared to the orbitals of the trans structure. The brightest transition of the cis conformer is shifted 13 nm towards smaller wavelengths compared to the trans structure. Just as for the trans conformer, we compare the geometries of the optimized ground and excited states as shown in Table S7 of the Supporting Information. It is interesting to note that, whereas the ground cis structure has a dihedral angle of circa  $32^\circ$ , the excited states become planar. Finally, we also note that for most values of  $\phi$ , a second peak is observed around 250–260 nm. However, no second peak is found for dihedral angles around  $90^\circ$ . This has been observed

earlier: the presence of two bands is an indication that the structure is not twisted, whereas only one band is visible in this region for a large twist.<sup>[80]</sup>

As already stated above, the main absorption peak mainly consists of a HOMO→LUMO transition for all dihedral angles. Therefore, these observations are in agreement with the well known fact that the HOMO-LUMO gap decreases when the conjugated system increases as shown in Figure S16 of the Supporting Information.

The same rotational analysis has been performed for linkers (3), (5)–(8) and their UV-Vis spectra are taken up in Figures S17, S18, S19, S20 and S21 respectively. All these spectra show the same qualitative behaviour, the main absorption peak fluctuates over a relatively large wavelength range up to 80 nm, but for some linkers, the global pattern can be different at some specific values of the dihedral angle.

We also performed some MD simulations from which snapshots are extracted which are used as input structures for TDDFT calculations.<sup>[20,36]</sup> The small spread in the dihedral angles results in a broadening of the main absorption peak as shown in Figure S22.

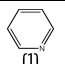
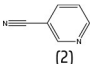
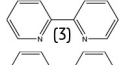
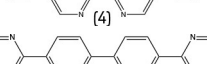
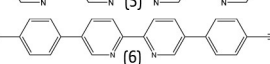
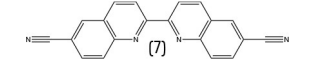
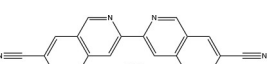
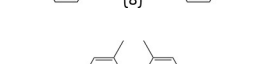
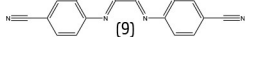
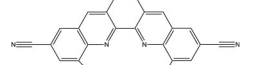
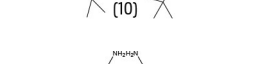
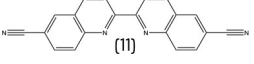
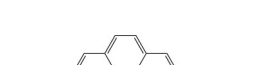
## 3.4.4. Other Ligands

Finally, we extend the study by a series of linkers (7)–(13) which might be interesting building blocks for CTF structures. Table 4 gives an overview of the energy of the main absorption peaks along with the dihedral angle of the optimized structure. For linkers (3)–(8), both the cis and trans conformers are studied. Experimental values are given in the last column.

First, we compare linkers (7) and (8) with the cis conformer of linker (4). They have similar dihedral angles, nevertheless, the shift of the position of the main absorption peak is rather large, *i.e.*, 47 nm and 65 nm respectively. This is because the conjugated  $\pi$ -system of linkers (7) and (8) is larger with respect

to linker (4) which results in a shift towards larger wavelengths. However, it is remarkable that although linkers (7) and (8) have a similar value of  $\phi_{cis}$  and only differ in the position of the two nitrogen atoms, their UV-Vis spectra reveal some specific discrepancies (Figure S30 in the Supporting Information). Both spectra exhibit three dominant peaks, but the position of the main absorption peak at the smallest excitation energy is shifted by 18 nm. They represent HOMO→LUMO excitations and their MOs are shown in Figures S23 and S24 of the Supporting Information. These orbitals are similar to those of naphthalene as predicted by Hückel's theory.<sup>[97]</sup> The contribution of the nitrogen atoms on the ring to the molecular orbital coefficients are reported in Table S8. The largest contributions

**Table 4.** Dihedral angle [°] and energy of the main absorption peak [nm] and [eV] between brackets for all linkers. Linkers (3)–(8) have both a cis and trans structure and  $E_{trans}$ ,  $E_{cis}$  and  $\phi_{cis}$  are reported whereas the other linkers only have one optimized structure for which  $E$  and  $\phi$  are given. Largest shift of the main absorption peak with respect to pyridine amounts to 271 nm and belongs to ligand 11. In the last column the experimental results are displayed. Calculations carried out at the B3LYP/6-31++G\*\* level of theory and with acetonitrile as solvent.

| Linker  | $E_{trans}$ | $E_{cis}$           | $\phi_{cis}$ | $E$                 | $\phi$ | $E_{exp}$ |
|---|-------------|---------------------|--------------|---------------------|--------|-----------|
| <br>(1)    |             |                     |              | 229(5.41)           | /      | 251(4.94) |
| <br>(2)    |             |                     |              | 240(5.17)           | /      | 264(4.70) |
| <br>(3)   | 270(4.59)   | 257(4.82)           | 34.2         |                     |        | 281(4.41) |
| <br>(4)  | 311(3.99)   | 298(4.16)           | 32.4         |                     |        | 301(4.12) |
| <br>(5)  | 353(3.51)   | 338(3.67)           | 33.3         |                     |        |           |
| <br>(6)  | 356(3.48)   | 340(3.65)           | 32.8         |                     |        | 323(3.84) |
| <br>(7)  | 377(3.29)   | 345(3.59)           | 34.2         |                     |        |           |
| <br>(8)  | 377(3.29)   | 266(4.66)           | 36.4         |                     |        |           |
|   |             | 275(4.51)–270(4.59) |              |                     |        |           |
| <br>(9)  |             |                     |              | 310(4.00)           | 112    |           |
| <br>(10) |             |                     |              | 252(4.92)           |        |           |
| <br>(11) |             |                     |              | 305(4.07)           | 106    |           |
| <br>(12) |             |                     |              | 258(4.81)           |        |           |
| <br>(13) |             |                     |              | 500(2.48)           | 158    |           |
|   |             |                     |              | 351(3.53)           |        |           |
|   |             |                     |              | 296(4.19)–285(4.35) |        |           |
|   |             |                     |              | 311(3.99)           | 180    |           |
|   |             |                     |              | 289(4.29)           |        |           |
|   |             |                     |              | 326(3.80)           | 180    |           |
|   |             |                     |              | 301(4.12)           |        |           |
|   |             |                     |              | 255(4.86)           |        |           |

are indicated in green and show that both the HOMO and LUMO of ligand (7) have a large contribution from the nitrogen atoms, whereas only the LUMO of ligand (8) has a significant contribution. The inclusion of nitrogen into the orbital results in a lowering of the orbital energy due to the larger electron negativity of nitrogen compared to carbon. For ligand (7), both the HOMO and LUMO decrease in energy, whereas for ligand (8), only the LUMO gets stabilized. Therefore, the HOMO-LUMO gap is smaller for ligand (8), *i.e.* 3.905 eV, than for ligand (7), *i.e.* 4.085 eV. This explains the observed shift in the main absorption peak for these linkers.

Second, we focus on linkers (7) and (9)–(11) which have more or less the same ring topology but differ in the number of side groups. The UV-Vis spectra are displayed in Figure 15. We can explain the position of the main absorption peak by accounting for the size of the conjugated  $\pi$ -system which is correlated to the dihedral angle. We observe that the more planar the structure is, *i.e.*,  $\phi$  is close to  $0^\circ$  or  $180^\circ$ , the more the peak shifts towards larger wavelengths. Ligands (9) and (10) show an optimized structure with a dihedral angle equal to  $112^\circ$  and  $106^\circ$  respectively, and are thus far from planar. Their main absorption peaks are clearly positioned at lower wavelengths than those in ligands (7) and (11). We found in Section 3.4.3 a shift of around 50 nm between planar and dihedral angles of  $90^\circ$  for linker (4). The shifts observed between linkers (7), (9) and (10) are of the same order of magnitude. However, for linker (11), we notice an absorption peak at 500 nm, isolated from the peaks of the other linkers which are situated in the range of 350 nm–200 nm. This significant shift toward larger

wavelengths cannot be explained by considering only the size of the  $\pi$ -system which is correlated to the dihedral angle, but can be explained by the presence of the electron-donating  $\text{NH}_2$  groups. Indeed, this linker has an extra occupied orbital situated on the  $\text{NH}_2$  group, which is higher in energy than occupied orbitals which are not situated on these groups. Therefore, we observe an extra transition for linker (11) at very high wavelengths. Compared to linker (1), the main absorption peak is shifted 271 nm towards larger wavelengths for linker (11).

Furthermore, it is also interesting to compare the *cis* structure of linker (4) and linker (12) shown in Figure S31 of the Supporting Information. As the latter has a larger conjugated  $\pi$ -system, we expect the peak to be situated at larger wavelengths. Indeed, we observe a shift between the peaks corresponding with a  $\pi_Q \rightarrow \pi_Q^*$  transition of 13 nm towards longer wavelengths. Remark that ligand (12) has a transition with higher oscillator strength at 289 nm.

Finally we also compare linkers (2) and (13) of which the UV-Vis spectra are shown in Figure 16. The shift of the main absorption peak, which is a  $\pi_Q \rightarrow \pi_Q^*$  transition for both linkers, amounts to 86 nm. Indeed, linker (13) is more  $\pi$ -electron deficient and has a larger  $\pi$ -system than linker (2). Furthermore, we notice that both linkers have a stronger excitation, at 221 nm and 255 nm respectively.

This shows that the position of the main absorption peak can be explained, and even tuned, by changing the size of the conjugated  $\pi$ -system, the amount of  $\pi$ -electron deficiency and by adding functional groups.

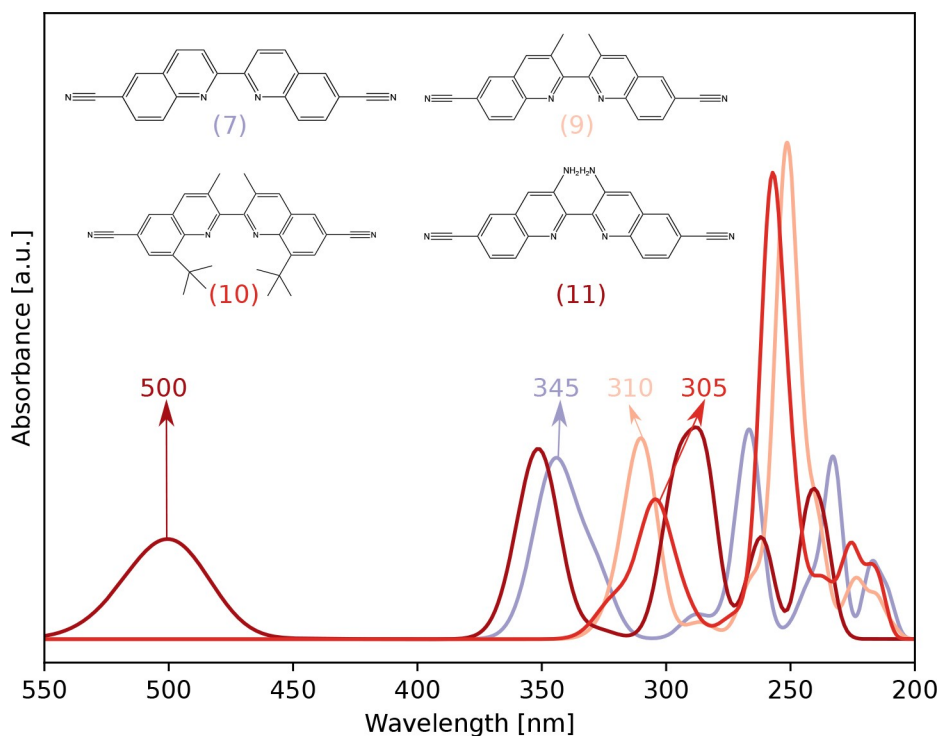


**Figure 15.** Theoretical UV-Vis spectra of ligands (7),(9), (10), and (11). Calculations carried out at the B3LYP/6-31 + G\*\* level of theory and with acetonitrile as solvent.

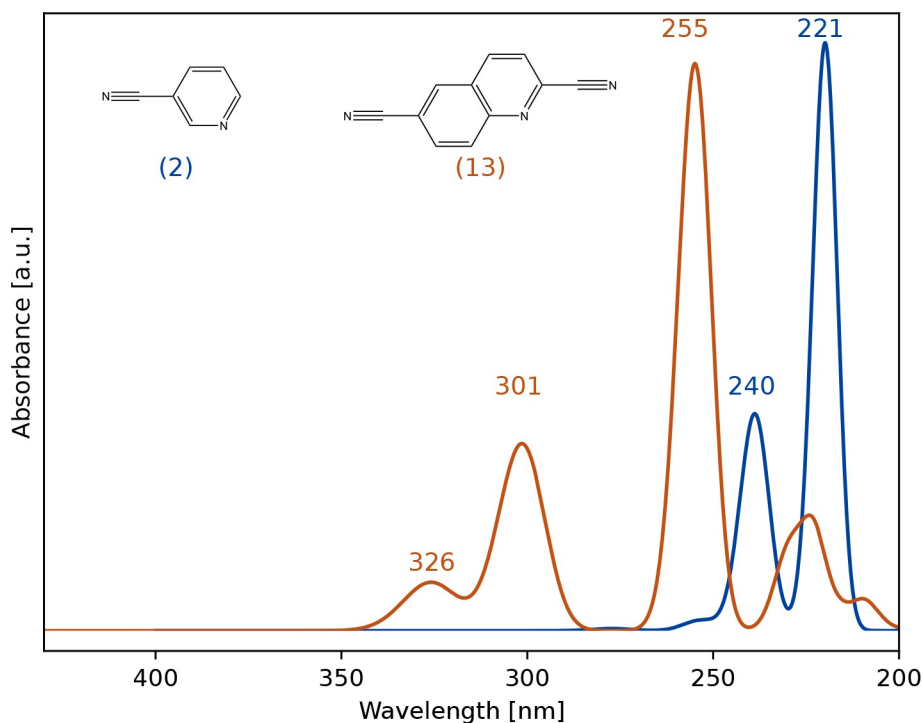


Figure 16. Theoretical UV-Vis spectra of ligands (2) and (13). Calculations carried out at the B3LYP/6-31++G\*\* level of theory and with acetonitrile as solvent.

For completeness, the orbitals contributing to the most important excitations of linkers (7)–(12) are shown in Figures S23, S24, S25, S26, S27, S28 and S29 of the Supporting Information. The UV-Vis spectra are shown in Figures 15 and 16 and Figures S30 and S31 of the Supporting Information. Furthermore, all singlet excitation energies along with the oscillator strength are listed in Table S9 of the Supporting Information for all linkers studied in this work.

## 4. Conclusions

We investigated, both experimentally and computationally, the structural and photophysical properties of various polypyridyl ligands which can be used to build CTFs. Therefore, we performed TDDFT calculations at the B3LYP/6-31++G\*\* level of theory and investigated the shift of the main absorption peak. We found that the larger the  $\pi$ -system and the higher its  $\pi$ -electron deficiency, the more the main absorption peak shifts to larger wavelengths. This can be achieved by adding aromatic rings, increasing the nitrogen content, or terminating the linker with electron withdrawing  $\text{CN}^-$  groups. Furthermore, we studied the influence of the dihedral angle, determined by the rotation about the central C–C bond, which is characteristic for all polypyridyl ligands under study in this work, on the UV-Vis spectrum. We found that the main absorption peak shifts to smaller wavelengths when the  $\pi$ -system decreases, which occurs when the dihedral angle is close to  $90^\circ$ . Furthermore, we showed that the position of the main absorption peak can be further shifted to larger wavelengths by increasing the nitrogen

content of the linker. The maximum shift can amount to 271 nm with respect to pyridine, which is sufficiently large to have a significant impact on the photophysical properties of the polypyridyl ligands. This broad range of shifts of the main absorption peak gives perspective in the modulation of the electronic structure by varying the ligands. Therefore, this study reveals how the optical properties of the CTF scaffold can be tuned by choosing the linkers.

## Acknowledgements

The authors acknowledge the Fund for Scientific Research Flanders (FWO) and the Research Board of Ghent University (BOF) through a Concerted Research Action (GOA) for funding. V.V.S. and L.D.B. acknowledge funding from the European Union's Horizon 2020 research and innovation program (consolidator ERC Grant Agreement No. 647755-DYNPOR (2015-2020)). The computational resources and services used in this work were provided by VSC (Flemish Supercomputer Center), funded by Ghent University, FWO, and the Flemish Government Department EWI.

## Conflict of Interest

The authors declare no conflict of interest.

**Keywords:** covalent triazine framework · photocatalysis · polypyridyl ligand · time-dependent functional theory · UV-Vis spectroscopy

- [1] C. Adamo, V. Barone, *J. Chem. Phys.* **1999**, *110*, 6158.
- [2] C. Adamo, D. Jacquemin, *Chem. Soc. Rev.* **2013**, *42*, 845–856.
- [3] U. I. E. Agency *International Energy Outlook 2016*.
- [4] H. B. Aiyappa, J. Thote, D. B. Shinde, R. Banerjee, S. Kurungot, *Chem. Mater.* **2016**, *28*, 4375–4379.
- [5] T. Banerjee, B. V. Lotsch, *Nat. Chem.* **2018**, *10*, 1175–1177.
- [6] A. M. Beale, S. D. M. Jacques, B. M. Weckhuysen, *Chem. Soc. Rev.* **2010**, *39*, 4656–4672.
- [7] A. D. Becke, *J. Chem. Phys.* **1993**, *98*, 5648.
- [8] A. Bolovinos, P. Tsekeris, J. Philis, E. Pantos, G. Andritsopoulos, *J. Mol. Spectrosc.* **1984**, *103*, 240–256.
- [9] G. A. Bowmaker, F. M. M. Hannaway, P. C. Junk, A. M. Lee, B. W. Skelton, A. H. White, *Austr. J. Chem.* **1988**, *51*, 331–336.
- [10] N. Burford, T. S. Cameron, K. N. Robertson, A. D. Phillips, H. A. Jenkins, *Chem. Commun.* **2000**, 2087–2088.
- [11] Z. L. Cai, J. R. Reimers, *J. Phys. Chem. A* **2000**, *104*, 8389.
- [12] J. U. Cameron, R. C. G. Killeen, *Cryst. Struct. Commun.* **1972**, *1*, 31–45.
- [13] M. Caricato, G. W. Trucks, M. J. Frisch, K. B. Wibler, *J. Chem. Theory Comput.* **2010**, *6*, 370.
- [14] M. E. Casida, C. Jamorski, K. C. Casida, D. R. Salahub, *J. Chem. Phys.* **1998**, *108*, 4439–4449.
- [15] J. D. Chai, M. Head-Gordon, *Phys. Chem. Chem. Phys.* **2008**, *10*, 6615–6620.
- [16] G. Chelucci, R. P. Thummel, *Chem. Rev.* **2002**, *102*, 3129–3170.
- [17] C. L. Cheng, D. S. N. Murthy, G. L. Ritchie, *J. Chem. Soc. Faraday Trans. 2* **1972**, *68*, 1679–1690.
- [18] S. Cogan, S. Zilberg, Y. Haase, *J. Am. Chem. Soc.* **2006**, *128*, 3335.
- [19] Z. Dega-Szafran, *Roc. Chem.* **1976**, *50*, 423.
- [20] A. Van Yperen-De Deyne, K. Hendrickx, L. Vanduyfhuys, G. Sastre, P. Van Der Voort, V. Van Speybroeck, K. Hemelsoet, *Theor. Chem. Acc.* **2016**, *135*.
- [21] S. Y. Ding, W. Wang, *Chem. Soc. Rev.* **2013**, *42*, 548–568.
- [22] E. V. Dose, L. J. Wilson, *Inorg. Chem.* **1978**, *17*, 2660–2666.
- [23] F. Egidi, M. Segado, H. Koch, C. Cappelli, V. Barone, *J. Chem. Phys.* **2014**, *141*, 224114.
- [24] M. J. Frisch, G. W. Trucks, H. B. Schlegel, G. E. Scuseria, M. A. Robb, J. R. Cheeseman, G. Scalmani, V. Barone, G. A. Petersson, H. Nakatsuji, X. Li, M. Caricato, A. V. Marenich, J. Bloino, B. G. Janesko, R. Gomperts, B. Mennucci, H. P. Hratchian, J. V. Ortiz, A. F. Izmaylov, J. L. Sonnenberg, D. Williams-Young, F. Ding, F. Lipparini, F. Egidi, J. Goings, B. Peng, A. Petrone, T. Henderson, D. Ranasinghe, V. G. Zakrzewski, J. Gao, N. Rega, G. Zheng, W. Liang, M. Hada, M. Ehara, K. Toyota, R. Fukuda, J. Hasegawa, M. Ishida, T. Nakajima, Y. Honda, O. Kitao, H. Nakai, T. Vreven, K. Throssell, Montgomery Jr., J. A., J. E. Peralta, F. Ogliaro, M. J. Bearpark, J. J. Heyd, E. N. Brothers, K. N. Kudin, V. N. Staroverov, T. A. Keith, R. Kobayashi, J. Normand, K. Raghavachari, A. P. Rendell, J. C. Burant, S. S. Iyengar, J. Tomasi, M. Cossi, J. M. Millam, M. Klene, C. Adamo, R. Cammi, J. W. Ochterski, R. L. Martin, K. Morokuma, O. Farkas, J. B. Foresman, D. J. Fox, **2016**, Gaussian 16 Revision B.01; Gaussian Inc. Wallingford CT.
- [25] R. Fukuda, M. Ehara, *J. Chem. Phys.* **2012**, *137*, 134304.
- [26] R. Fukuda, M. Ehara, *Phys. Chem. Chem. Phys.* **2013**, *15*, 17426–17434.
- [27] R. Fukuda, M. Ehara, *J. Chem. Theory Comput.* **2013**, *9*, 470–480.
- [28] R. Fukuda, M. Ehara, H. Nakatsuji, *J. Chem. Phys.* **2010**, *133*, 144316.
- [29] A. Göller, U. W. Grummt, **2000**, *321*, 399–405.
- [30] L. Goodman, *J. Mol. Spectrosc.* **1961**, *6*, 109.
- [31] S. Grimme, J. Antony, S. Ehrlich, H. Krieg, *J. Chem. Phys.* **2010**, *132*, 154104.
- [32] G. H. Gunasekar, K. Park, H. H. Jeong, K. D. Jung, K. Park, S. Yoon, *Catalysts* **2018**, *8*, 295.
- [33] D. C. Harris, M. D. Bertolucci, *Symmetry and spectroscopy: an introduction to vibrational and electronic spectroscopy*. Oxford University Press, **1978**.
- [34] T. M. Henderson, A. F. Izmaylov, G. Scalmani, G. E. Scuseria, *J. Chem. Phys.* **2009**, *131*, 044108.
- [35] C. H. Hendon, J. Bonnefoy, E. A. Quadrelli, J. Canivet, M. B. Chambers, G. Rousse, A. Walsh, M. Fontecave, C. Mellot-Draznieks, *Chem. Eur. J.* **2016**, *22*, 3713–3718.
- [36] K. Hendrickx, D. E. P. Vanpoucke, K. Leus, K. Lejaeghere, A. Van Yperen-De Deyne, V. Van Speybroeck, P. Van Der Voort, K. Hemelsoet, *Inorg. Chem.* **2015**, *54*, 10701–10710.
- [37] C. C. Hou, T. T. Li, S. Cao, Y. Chen, W. F. Fu, *J. Mater. Chem. A* **2015**, *3*, 10386–10394.
- [38] S. Hug, M. B. Mesch, H. Oh, N. Popp, M. Hirscher, J. Senker, B. V. Lotsch, **2014**, *J. Mater. Chem. A*, 5928–5936.
- [39] S. Hug, L. Stegbauer, H. Oh, M. Hirscher, B. V. Lotsch, *Chem. Mater.* **2015**, *27*, 8001–8010.
- [40] S. Hug, M. E. Tauchert, S. Li, U. E. Pachmayr, B. V. A. Lotsch, *J. Mater. Chem.* **2012**, *22*, 13956–13964.
- [41] P. A. Jacobs, M. Dusselier, B. F. Sels, *Angew. Chem. Int. Ed.* **2014**, *53*, 8621–8626; *Angew. Chem.* **2014**, *126*, 8765–8770.
- [42] D. Jacquemin, E. A. Perpète, I. Ciofini, C. Adamo, R. Valero, Y. Zhao, D. G. Truhlar, *J. Chem. Theory Comput.* **2010**, *6*, 2071–2085.
- [43] D. Jacquemin, V. Wathelet, E. A. Perpète, C. Adamo, *J. Chem. Theory Comput.* **2009**, *5*, 2420–2435.
- [44] E. M. Johnson, R. Haiges, S. C. Marinescu, *ACS Appl. Mater. Interfaces* **2018**, *10*, 37919–3792.
- [45] J. Kalenik, Z. Pawelka, *J. Mol. Liq.* **2005**, *121*, 63–68.
- [46] K. Kalyanasundaram, *Coord. Chem. Rev.* **1982**, *46*, 159–244.
- [47] M. D. Kärkäs, J. A. J. Porco, C. R. Stephenson, *Chem. Rev.* **2016**, *116*, 9683–9747.
- [48] F. Labat, P. P. Laine, I. Ciofini, C. Adamo, *Chem. Phys. Lett.* **2006**, *417*, 445–451.
- [49] A. D. Laurent, D. Jacquemin, *Int. J. Quantum Chem.* **2013**, *113*, 2019–2039.
- [50] C. Lee, W. Yang, R. G. Parr, *Phys. Rev. B* **1988**, *37*, 785–789.
- [51] C. Lee, W. Yang, R. G. Parr, *Phys. Rev. B* **1988**, *37*, 785.
- [52] A. Lipka, H. Wunderlich, *Z. Naturforsch. B* **1980**, *35*, 1548.
- [53] M. S. Lohse, T. Bein, *Adv. Funct. Mater.* **2018**, *28*, 1705553.
- [54] W. A. Maza, A. J. Morris, *J. Phys. Chem. C* **2014**, *118*, 8803–8817.
- [55] L. L. Merritt, E. D. Schroeder, *Acta Crystallogr.* **1956**, *9*, 801–804.
- [56] T. D. Meyer, I. Steyaert, K. Hemelsoet, R. Hoogenboom, V. Van Speybroeck, K. De Clerck, *Dyes Pigm.* **2016**, *124*, 249–257.
- [57] B. Miehlisch, A. Savin, H. Stoll, H. Preuss, *Chem. Phys. Lett.* **1989**, *157*, 200–206.
- [58] F. Muniz-Miranda, L. De Bruecker, A. De Vos, F. Vanden Bussche, C. V. Stevens, P. Van Der Voort, K. Lejaeghere, V. Van Speybroeck, *J. Phys. Chem. A* **2019**, *123*, 6854–6867.
- [59] F. Muniz-Miranda, M. C. Menziani, A. Pedone, *J. Phys. Chem. C* **2014**, *118*, 7532–7544.
- [60] K. Nakamoto, *J. Phys. Chem.* **1960**, *64*, 1420–1425.
- [61] J. M. R. Narayanam, C. R. J. Stephenson, *Chem. Soc. Rev.* **2011**, *40*, 102–113.
- [62] M. Nooijen, R. J. Bartlett, *J. Chem. Phys.* **1997**, *106*, 6441.
- [63] L. Oresmaa, M. Haukka, P. Vainiotalo, T. A. Pakkanen, *J. Org. Chem.* **2002**, *67*, 8216–8219.
- [64] M. Pagliai, G. Mancini, I. Carnimeo, N. D. Mitri, V. Barone, *J. Comb. Chem.* **2017**, *38*, 319–335.
- [65] R. Palkovits, M. Antonietti, A. T. P. Kuhn, F. Schüth, *Angew. Chem. Int. Ed.* **2009**, *48*, 6909–6912.
- [66] K. Park, G. H. Gunasekar, N. Prakash, K. D. Jung, S. A. Yoon, *ChemSusChem* **2015**, *8*, 3410–3413.
- [67] J. P. Perdew, A. Ruzsinszky, J. Tao, V. N. Staroverov, G. E. Scuseria, G. I. Csonka, *J. Chem. Phys.* **2005**, *123*, 062201.
- [68] D. A. Popov, J. M. Luna, N. M. Orchanian, R. Haiges, C. A. Downes, S. C. Marinescu, *Dalton Trans.* **2018**, *47*, 17450–17460.
- [69] C. K. Prier, D. A. Rankic, D. W. MacMillan, *Chem. Rev.* **2013**, *113*, 5322–5363.
- [70] A. Primo, H. Garcia, *Chem. Soc. Rev.* **2014**, *43*, 7548–7561.
- [71] S. M. J. Rogge, A. Bavykina, J. Hajek, H. Garcia, A. I. Olivios-Suarez, A. Sepúlveda-Escribano, A. Vimont, G. Clet, P. Bazin, F. Kapteijn, M. Daturi, E. V. Ramos-Fernandez, F. X. L. I. Xamena, V. Van Speybroeck, J. Gascon, *Chem. Soc. Rev.* **2017**, *46*, 3134–3184.
- [72] E. Runge, E. K. U. Gross, *Phys. Rev. Lett.* **1984**, *52*, 997–1000.
- [73] S. P. A. Sauer, M. Schreiber, M. R. Silva-Junior, W. Thiel, *J. Chem. Theory Comput.* **2009**, *5*, 555–564.
- [74] M. Schreiber, M. R. Silva-Junior, S. P. A. Sauer, W. Thiel, *J. Chem. Phys.* **2008**, *128*, 134110.
- [75] D. M. Schultz, T. P. Yoon, *Science* **2014**, *343*, 1239176.
- [76] A. G. Slater, A. I. Cooper, *Science* **2015**, *348*, aaa8075.
- [77] V. N. Staroverov, G. E. Scuseria, J. Tao, J. P. Perdew, *J. Chem. Phys.* **2003**, *119*, 12129.



- [78] L. Stegbauer, K. Schwinghammer, B. V. Lotsch, *Chem. Sci.* **2014**, *5*, 2789–2793.
- [79] L. A. Summers, *Adv. Heterocycl. Chem.* **1984**, *35*, 281.
- [80] H. Suzuki, *Bull. Chem. Soc. Jpn.* **1959**, *32*, 1340–1350.
- [81] N. Tahir, C. Krishnaraj, K. Leus, P. Van Der Voort, *Polymer* **2019**, *11*.
- [82] N. Tahir, F. Muniz-Miranda, J. Everaert, P. Tack, T. Heugebaert, K. Leus, L. Vincze, C. V. Stevens, V. Van Speybroeck, P. Van Der Voort, *J. Catal.* **2019**, *371*, 135–143.
- [83] N. Tahir, G. Wang, Y. Onyshchenko, N. D. Geyter, K. Leus, R. Morent, P. Van Der Voort, *J. Catal.* **2019**, *375*, 242–248.
- [84] K. Takanabe, *ACS Catal.* **2017**, *7*, 8006–8022.
- [85] H. Takeda, M. Ohashi, Y. Goto, T. Ohsuna, T. Tani, S. Inagaki *Adv. Funct. Mater.*, **2016**, *26*, 5068–5077.
- [86] J. Tao, J. P. Perdew, V. N. Staroverov, G. E. Scuseria, *Phys. Rev. Lett.* **2003**, *91*, 146401.
- [87] J. Tomasi, B. Mennucci, R. Cammi, *Chem. Rev.* **2005**, *105*, 2999–3094.
- [88] W. Tu, Y. Xu, S. Yin, R. Xu, *Adv. Mater.* **2018**, *30*, 1707582.
- [89] J. VandeVondele, M. Krack, F. Mohamed, M. Parrinello, T. Chassaing, J. Hutter, *Comput. Phys. Commun.* **2005**, *167*, 103–128.
- [90] A. De Vos, K. Lejaeghere, F. Muniz-Miranda, C. V. Stevens, P. Van Der Voort, V. Van Speybroeck, *J. Mater. Chem. A* **2019**, *7*, 8433–8442.
- [91] V. S. Vyas, F. Haase, L. Stegbauer, G. Savasci, F. Podjaski, C. Ochsenfeld, B. V. Lotsch, *Nat. Commun.* **2015**, *6*, 8508.
- [92] I. C. Walker, M. H. Palmer, A. Hopkirk, *Chem. Phys.* **1990**, *141*, 365.
- [93] J. Wan, M. E. M. Hada, H. Nakatsuji, *J. Chem. Phys.* **2001**, *114*, 5117.
- [94] B. M. Weckhuysen, *ChemSusChem* **2013**, *6*, 1559–1563.
- [95] T. Yanai, D. P. Tew, N. C. Handy, *Chem. Phys. Lett.* **2004**, *393*, 51–57.
- [96] D. Yang, S. O. Odoh, T. C. Wang, O. K. Farha, J. T. Hupp, C. J. Cramer, L. Gagliardi, B. C. Gates, *J. Am. Chem. Soc.* **2015**, *5*, 7391–7396.
- [97] K. Yoshizawa, T. Tada, A. Staykov, *JACS* **2008**, *130*, 9406–9413.
- [98] Y. Zhao, D. G. Truhlar, *Theor. Chem. Acc.* **2008**, *120*, 215–241.

---

Manuscript received: July 10, 2020

Revised manuscript received: September 7, 2020

Accepted manuscript online: September 11, 2020

Version of record online: October 28, 2020